2014

Numerical Simulation on the Opening Delay of a Discharge Reed Valve in Compressors

Fumitaka Yoshizumi
Toyota Central R&D Labs., Inc., fyoshi@mosk.tytlabs.co.jp

Yasuhiro Kondoh
Toyota Central R&D Labs., Inc., ykondoh@fldlab.tytlabs.co.jp

Takahiro Moroi
Toyota Industries Co., takahiro.moroi@mail.toyota-shokki.co.jp

Shinji Tamano
Nagoya Institute of T, tamano.shinji@nitech.ac.jp

Yohei Morinishi
Nagoya Institute of T, morinishi.yohei@nitech.ac.jp

Numerical Simulation on the Opening Delay of a Discharge Reed Valve in Compressors

Fumitaka YOSHIZUMI[1]*, Yasuhiro KONDOH[1], Takahiro MOROI[2], Shinji TAMANO[3], Yohei MORINISHI[3]

[1]Toyota Central R & D Labs., Inc.,
Nagakute, Aichi, Japan
* fyoshi@mosk.tytlabs.co.jp, ykondoh@fldlab.tytlabs.co.jp

[2]Toyota Industries Corporation, Compressor Division,
Kariya, Aichi, Japan
takahiro.moroi@mail.toyota-shokki.co.jp

[3]Nagoya Institute of Technology, Dept. of Engineering Physics, Electronics and Mechanics
Nagoya, Aichi, Japan
tamano.shinji@nitech.ac.jp, morinishi.yohei@nitech.ac.jp

* Corresponding Author

ABSTRACT

The opening delay of a discharge reed valve for compressors caused by the stiction force of the oil film between the reed and the valve seat is investigated. The coupling simulation algorithm including models of cavitation in the oil film is developed. The two-dimensional oil film pressure distribution is obtained by solving numerically the Reynolds' equation through the finite volume method. On the model of cavitation in the oil film, in addition to the case in which cavitation is not taken into account, two cavitation models are tested; the static cavitation model (Reynolds' condition) in which the minimum oil pressure is set to absolute zero, and the dynamic cavitation model in which the oil film pressure can fall to the absolute negative (tensile in the liquid) due to the direct simulation of the bubble expansion. In order to check the validity, the numerical simulation is performed under a condition of a model experiment. Comparisons on the opening delay time between simulation results and the experimental result show that the static cavitation model gives the earlier delay time than that in the experiment, and the dynamic cavitation model which simulates the absolute negative pressure in the oil film reproduces quantitatively the experimental delay time. Based on the simulation result throught the dynamic cavitation model, the mechanism of the oil film rupture (valve opening) is discussed.

1. INTRODUCTION

The reed valve is widely used in the discharge part of refrigerant compressors. The reed valve consists of a reed (a thin plate) and a valve seat. The valve opens and closes automatically depending on the pressure difference between the cylinder bore and chambers. Ideally, the valve starts to open when the bore pressure becomes equal to the chamber pressure. However, there exists the opening delay in real valves which can bring about an extreme over-compression and subsequent losses. The opening delay of reed valves is mainly caused by the stiction force of the oil film between the reed and the valve seat. The simulation model to predict the stiction behavior and the opening delay time is desired to develop valves with the lower loss.

The authors have developed a model experiment setup and carried out a simultaneous observation of the reed

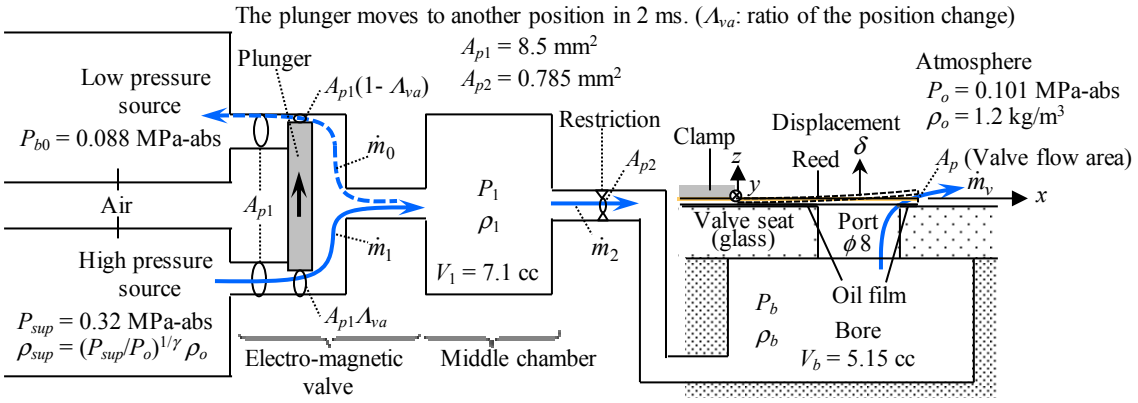

Figure 1: The whole simulation model of the experimental setup

deformation and the oil film (Yoshizumi *et al*., 2012) .They have observed that the oil film thickness increases during stiction and the cavitation region spreads in the oil film just before the oil film rupture. It may be required to simulate the expansion of cavitation bubbles in order to predict the opening delay time length (time at which the oil film ruptures) accurately. Oil film models based on the basic equation for squeeze films, i.e., the Reynolds' equation, are developed by some researchers (Bauer, F., 1990, Khalifa, H. E., Liu, X., 1998, Bukac, H., 2002, Pizarro-Recabarren R. A. *et al*., 2012). However, validity of models is not clear yet since all of the models do not simulate directly the cavitation bubble and then it is not clear how much the oil film pressure falls before the oil film rupture.

In this study, the coupling simulation algorithm including models of cavitation in the oil film is developed. Particularly, a cavitation model in which the bubble expansion is directly simulated (dynamic cavitation model) is developed as well as the conventional static cavitation model (Reynolds' condition). In order to check the validity, the numerical simulation using each cavitation model is performed under a condition of the model experiment in authors' previous work (Yoshizumi *et al*., 2012).

2. SIMULATION MODEL

The simulation model for the experimental setup is developed to compare results and check validity. The whole simulation model is shown in Figure 1. The model consists of the reed deformation, the gas (air in the experiment) flow and the oil film with cavitation.

2.1 Reed deformation

The reed deformation is modeled by FEM (Finite Element Method) using shell elements in order to express the two-dimensional bending deformation along the reed plane. The equation of motion is expressed in a matrix form as,

$$[M]\{\ddot{X}\}+[C]\{\dot{X}\}+[K]\{X\}=\{F_g\}+\{F_{oil}\}. \tag{1}$$

This matrix form is expanded to equations of natural modes (modal equations). Natural modes are obtained by the eigenvalue analysis of the free problem where the right hand side of Equation (1) is replaced by the zero vector. Each modal equation is integrated by the Newmark-β method individually.

2.2 Gas flow and the gas force on the valve

The gas flow is assumed to be expressed by a thermal lumped-parameter system model. Both in the middle chamber and in the bore, the thermal process is assumed to be internal reversible process. Furthermore the whole pneumatic system is assumed to be isentropic. Then, the relation between pressures and densities in the system is expresses by

$$P_{sup}/\rho_{sup}{}^{\gamma} = P_1/\rho_1{}^{\gamma} = P_b/\rho_b{}^{\gamma} = P_o/\rho_o{}^{\gamma} = \text{const.}. \tag{2}$$

From both Equation (2) and the equation of state for the ideal gas, equations for pressures in the middle chamber and the bore are expressed as follows,

$$\dot{P}_1 = -[\gamma P_1/(\rho_1 V_1)](\dot{m}_2 - \dot{m}_1 + \dot{m}_0), \tag{3}$$

$$\dot{P}_b = -[\gamma P_b/(\rho_b V_b)](\dot{m}_v - \dot{m}_2). \tag{4}$$

These pressure equations are integrated by the Crank-Nicolson method. The mass flow rates at paths are expressed as follows,

$$\dot{m}_0 = C_{d0} A_{p1}(1 - \Lambda_{va})\sqrt{2\rho_1 P_1} f_Q(P_{b0}/P_1), \tag{5}$$

$$\dot{m}_1 = C_{d1} A_{p1} \Lambda_{va} \sqrt{2\rho_{sup} P_{sup}} f_Q(P_1/P_{sup}), \tag{6}$$

$$\dot{m}_2 = C_{d2} A_{p2} \sqrt{2\rho_1 P_1} f_Q(P_b/P_1), \tag{7}$$

$$\dot{m}_v = C_d A_p \sqrt{2\rho_b P_b} f_Q(P_o/P_b), \tag{8}$$

where

$$f_Q(\Lambda_p) = \begin{cases} \sqrt{[\gamma/(\gamma-1)][\Lambda_p^{2/\gamma} - \Lambda_p^{(\gamma+1)/\gamma}]} & \cdots\cdots \ [(\gamma+1)/2]^{\gamma/(1-\gamma)} \le \Lambda_p \le 1, \\ \sqrt{[\gamma/(\gamma+1)][2/(\gamma+1)]^{2/(\gamma-1)}} & \cdots\cdots \ 0 \le \Lambda_p \le [(\gamma+1)/2]^{\gamma/(1-\gamma)} \end{cases}. \tag{9}$$

The flow area of the reed valve, A_p, changes according to the situation of the blow-by (oil film rupture) in the seal (oil film around the port) as shown in the Sec. 2.3 [Equation (21)], and A_p is zero before the oil film rupture. The gas force on the reed is expressed as the sum of the force by the pressure difference between front and back surfaces, F_{gp}, the steady fluid dynamic force, $F_{gsteady}$, and the unsteady fluid dynamic force, $F_{gunsteady}$. Only while the valve opens and the gas flows, $F_{gsteady}$ and $F_{gunsteady}$ act.

$$F_g = F_{gp} + F_{gsteady} + F_{gunsteady}, \tag{10}$$

$$F_{gp} = (\pi D_p^{\,2}/4)(P_b - P_o), \tag{11}$$

$$F_{gsteady} = -\dot{m}_v u_v \xi_v \cos\Theta_v = -[\dot{m}_v^{\,2}/(C_d A_p \rho_v)]\ \xi_v \cos\Theta_v, \tag{12}$$

$$F_{gunsteady} = -\ell_d \ddot{m}_v, \tag{13}$$

where $\rho_v = \rho_o$ under $[(\gamma+1)/2]^{\gamma/(1-\gamma)} \leqq P_o/P_b$ and $\rho_v = [(\gamma+1)/2]^{1/(1-\gamma)}\rho_b$ under $P_o/P_b < [(\gamma+1)/2]^{\gamma/(1-\gamma)}$. In the numerical procedure, F_g is discretized to lumped forces on nodes on the port of the FEM reed model. In order to obtain the initial gas flow condition at $t = 0$ ($P_b = P_o$) of the whole coupling simulation, the gas flow simulation ($A_p = 0$) before $P_b = P_o$ is executed beforehand.

2.3 Oil film pressure equation

The oil film model and cavitation bubble model are shown in Figure 2. The oil film pressure is expressed by the Reynolds' equation with the averaged flow model (Patir, N., Cheng, H. S., 1978) for the surface roughness as,

$$\frac{\partial}{\partial x}\left(\frac{\phi_x \rho h^3}{12\eta}\frac{\partial P_{oil}}{\partial x}\right) + \frac{\partial}{\partial y}\left(\frac{\phi_y \rho h^3}{12\eta}\frac{\partial P_{oil}}{\partial y}\right) = \frac{\partial \rho \bar{h}_T}{\partial t}, \tag{14}$$

where

$$\bar{h}_T = \int_{-h}^{\infty}(h + z_r) f_r(z_r) dz_r, \tag{15}$$

$$\rho = (1-\alpha)\rho_{oil} + \alpha\rho_g \cong (1-\alpha)\rho_{oil}, \tag{16}$$

$$\alpha = (4/3)N\pi r_b^{\,3}/h. \tag{17}$$

Here the right hand side of Equation (14) is approximated as follows,

$$\frac{\partial \rho \bar{h}_T}{\partial t} = \rho_{oil}\frac{\partial \bar{h}_T}{\partial t}\left[1 - \left(\frac{\partial \alpha \bar{h}_T}{\partial t}\Big/\frac{\partial \bar{h}_T}{\partial t}\right)\right] \cong \rho_{oil}\frac{\partial \bar{h}_T}{\partial t}\left[1 - \left(\frac{\partial \alpha h}{\partial t}\Big/\frac{\partial h}{\partial t}\right)\right]. \tag{18}$$

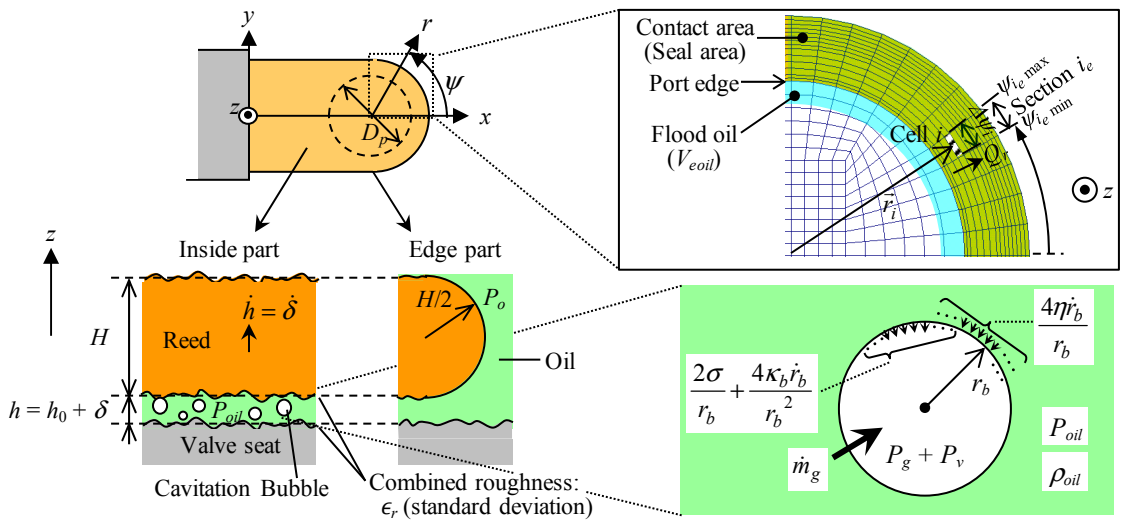

Figure 2: Oil film model and cavitation bubble model

Substituting Equation (16) into the left-hand side of Equation (14) and substituting Equation (18) with Equation (17) into the right-hand side of Equation (14) yield

$$\frac{\partial}{\partial x}\left[\frac{\phi_x(1-\alpha)h^3}{12\eta}\frac{\partial P_{oil}}{\partial x}\right]+\frac{\partial}{\partial y}\left[\frac{\phi_y(1-\alpha)h^3}{12\eta}\frac{\partial P_{oil}}{\partial y}\right]=\beta\frac{\partial\bar{h}_T}{\partial t}, \tag{19}$$

where β is the volume rate fraction for liquid written as,

$$\beta=1-\left(4N\pi r_b^{\,2}\dot{r}_b/\dot{h}\right). \tag{20}$$

The equation (19) is solved through FVM (Finite Volume Method). The FVM mesh is identical to the FEM mesh for the reed deformation mentioned in the Sec. 2.1.

The flow area of the reed valve, A_p in Equation (8), is given by the integration of the valve lift, h (= h_0 + δ), along the port edge circumference. The integration is executed numerically in each circumference section divided by FVM mesh nodes on the port edge as follows,

$$A_p=\sum_{i_e}A_{pi_e}, \tag{21}$$

$$A_{pi_e}=\begin{cases}\int_{\psi_{i_e\,min}}^{\psi_{i_e\,max}}(h_0+\delta)\big|_{r=D_p/2}(D_p/2)d\psi & \cdots\cdots \text{ All cells in } \psi_{i_e\,min}\le\psi\le\psi_{i_e\,max} \text{ are under blow - by,}\\ 0 & \cdots\cdots \text{ Not all cells in } \psi_{i_e\,min}\le\psi\le\psi_{i_e\,max} \text{ are under blow - by.}\end{cases} \tag{22}$$

where i_e is the section identity and the circumference angle (ψ) range of the section i_e is $\psi_{i_emin}\leqq\psi\leqq\psi_{i_emax}$. If not all cells (elements) of FVM ($r\ge D_p/2$) in the circumference section i_e are under blow-by, the flow area of section i_e (A_{pi_e}) is set to zero. In this paper, the blow-by condition of each cell is determined as follows (the subscript i means the cell i),

$$\int_0^t Q_{ri}dt>\left(\frac{\Delta\psi_i}{2\pi}\right)V_{eoil}\ \rightarrow \text{Cell } i \text{ is under blow-by.} \tag{23}$$

where $\Delta\psi_i$ is the ψ range of the cell i.The left hand side of Equation (23), that is, the accumulated flow volume (the time integration of the flow rate), is calculated by

$$\int_0^t Q_{ri}dt\cong-\int_0^t\frac{(1-\alpha_i)h_i^{\,3}}{12\eta}(\nabla P_{oil})_i\cdot\vec{r}_i\Delta\psi_i dt\quad(\phi_x=\phi_y\cong1), \tag{24}$$

where $\vec{r}_i$ is the position vector whose base point is the center of the port.

2.4 Bubble expansion equation

The bubble shape is assumed a sphere ($h \geq 2r_b$) or an oblate spheroid ($h < 2r_b$), and for the both cases, the bubble expansion is assumed to be governed by the equation of a spherical bubble, i.e., the Rayleigh-Plesset equation,

$$\ddot{r}_b r_b + \left(\frac{3}{2}\right)\dot{r}_b^{\,2} = \frac{1}{\rho_{oil}}\left(P_g + P_v - P_{oil} - \frac{2\sigma}{r_b} - \frac{4\eta\dot{r}_b}{r_b} - \frac{4\kappa_b\dot{r}_b}{r_b^{\,2}}\right). \tag{25}$$

In the right hand side of Equation (25), the surface dilatational viscosity (Natsumeda and Someya, 1990) is considered as the last term. The order of the inertial force of the left hand side is 10^{-5} of that of the sum of viscous terms (the fifth and the last terms of the right hand side), and omitting the left hand side of Equation (25) gives,

$$\dot{r}_b = \frac{r_b}{4[\eta + (\kappa_b / r_b)]}\left(P_g + P_v - P_{oil} - \frac{2\sigma}{r_b}\right) \quad (r_b > r_{bmin}). \tag{26}$$

The initial value of P_g, P_{g0}, is given by $P_{g0} = P_{cav\ onset} - P_v + (2\sigma / r_{b0})$.The thermal process in a bubble is assumed to be a polytropic process ($P_g / \rho_g^{\nu_{gb}} = \text{const}$, ρ_g: the density of the gas in the bubble). From this assumption and the equation of state ($P_g = \rho_g R_g T_g$), the equation of the pressure in a bubble is given by

$$\dot{P}_g = -(\nu_{gb} P_g / V_g)\dot{V}_g + (\nu_{gb} P_g / m_g)\dot{m}_g \quad (r_b > r_{bmin}), \tag{27}$$

where

$$V_g = (4/3)\pi r_b^{\,3}. \tag{28}$$

The mass diffusion rate of the dissolved gas in the oil is expresses as follows (Yamaguchi *et al*., 1983),

$$\dot{m}_g = [4\pi r_b^{\,2} \Gamma \chi_g / (R_g r_b)]\left[(P_{g0}/T_{g0}) - (P_g / T_g)\right] \quad (r_b > r_{bmin}). \tag{29}$$

The quatities of the bubble (r_b, P_g, m_g, T_g) are assigned to each cell in the FVM mesh, respectively. In the simulation, $\dot{r}_b$, $\dot{P}_g$, and $\dot{m}_g$ are integrated by the forward (explicit) Euler scheme, and r_b has the minimum value, r_{bmin},

$$\dot{r}_b = 0, \quad \dot{P}_g = 0, \quad \dot{m}_g = 0 \quad \text{at} \quad r_b = r_{bmin}. \tag{30}$$

2.5 Coupling method and the simulation condition

The equations of the reed [Equation (1)], the gas flow [Equations (3) and (4)] and the oil film equation [Equation (19)] are coupled by the iterative partitioned coupling algorithm to secure the numerical stability for the time step procedure. The detailed flow chart of the algorithm is shown in Yoshizumi *et al*. (2013a).

In relation to the oil film pressure, three cavitation models are tested.

- Model "***n***": non cavitation model. Cavitation in the oil film is not taken into account. The oil film equation [Equation (19)] is solved under $\alpha = 0$, $\beta = 1$ and without the minimum limit of P_{oil}.
- Model "***s***": static cavitation model (the Reynolds' condition). The oil film equation [Equation (19)] is solved under $\alpha = 0$, $\beta = 1$ and the minimum limit of P_{oil} (P_{cav}) which is set to absolute zero.
- Model "***d***": dynamic cavitation model. The oil film equation [Equation (19)] is solved under coupling with the bubble equation [Equations (26)-(30)]. The oil film pressure at which the bubble growth onsets, $P_{cav\ onset}$, is set to absolute zero to simulate the absolute negative pressure in the oil film. In each cell in the FVM mesh, before P_{oil} falls to the absolute zero, the bubble does not expand and Equation (19) is soloved under $\alpha = 0$, $\beta = 1$. The aritificial minimum limit of P_{oil} is not set.

In Model "***d***", in the integration of $\dot{r}_b$ and the calculation of β [Equation (20)], the 2nd order low-pass filter (the cutoff frequency, f_c, is 10 kHz) is applied to $\dot{r}_b$ obtained from Equation (26) in order to improve the numerical stability in the time step procedure. The effect of the filter on the opening delay time is considered to be small, since the change in f_c brings only +0.14 ms change (f_c = 5 kHz) or –0.04 ms change (f_c = 50 kHz) in the start time of the oil film rupture in Figure 5 (t_{rup}).

The simulation condition is shown in Table 1 as well as Figure 1. The FEM (FVM) mesh of the reed is shown in Figure 3. In consideration of the rubber sheet being inserted into the root clamp part, the fixed end is retreating 1 mm in the model (The distance between the fixed end and the center of the port is 13 mm.). MSC/Nastran 2008r1 is

Table 1: Simulation condition

Reed					
H	0.38 mm	V_{eoil}	5 mm^3**	R_g	288.7 J/(kg·K)
E_{reed}	2.1×10^{11} Pa	γ	1.4	r_{b0}	1.25 μm**
ν_{reed}	0.3	Θ_v	90 °	r_{bmin}	$r_{b0}-0.001$ μm
ρ_{reed}	7.8×10^3 kg/m^3	Oil film		T_{g0}	293 K
ζ_j	0.001	h_0	1 μm*	Γ	1×10^{-9} m^2/s**
Gas flow		P_{cav}	$-\infty$ (***n***)	κ_b	7.85×10^{-5} kg/s**
C_d	0.7	P_{cav}	0 MPa-abs (***s***)	ν_{gb}	1
C_{d0}	1	ϵ_r	0.2 μm	ρ_{oil}	9.9×10^2 kg/m^3
C_{d1}	1	η	0.085 Pa·S	σ	0.03 N/m
C_{d2}	0.64	Cavitation bubble (***d***)		χ_g	0.1**
D_p	8 mm	N	1×10^{10} m^{-2}**	Time step increment, Δt	
ℓ_d	16 mm	$P_{cav\ onset}$	0 MPa-abs**	$\Delta t \leqq$	1×10^{-7} s (***n***)(***s***)
		P_v	0 MPa-abs	$\Delta t \leqq$	1×10^{-9} s (***d***)

E_{reed}, ν_{reed} and ρ_{reed} are the Young' s modulus, the Poisson' s ratio and the density of the reed (steel) respectively.

*: assumed initial oil film thickness in the inside part (see Figure 2). **: assumed.

(***n***): non cavitation model, (***s***): static cavitation model, (***d***): dynamic cavitation model.

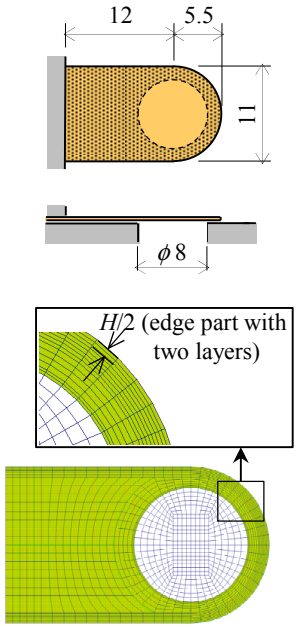

Figure 3: Valve configuration and FEM (FVM) mesh

used in the eigenvalue analysis of the reed, and six symmetric modes (natural frequencies ranges from 1.08 kHz to 35.2 kHz.) are incorporated into the modal expansion of the equation of motion for the reed [Equation (1)]. In Table 1, bubble parameters (N, r_{b0}, κ_b) in Model "***d***" are set by trial-and-error so that the opening delay time might suit the experiment. The initial oil film thickness, h_0, is set to 1 μm in light of the actual roughness, ϵ_r.

3. RESULTS

The bore pressures, P_b, and the reed displacements on the port, δ_p, through simulations using three cavitation models are shown in Figure 4 with the experimental result. The opening delay time by Model "***n***" is much longer than that in the experiment. The delay time by Model "***s***" is shorter than that in the experiment, and only Model "***d***" can reproduce the experimental delay time quantitatively. Figure 5 shows distributions and transients (at a node on the

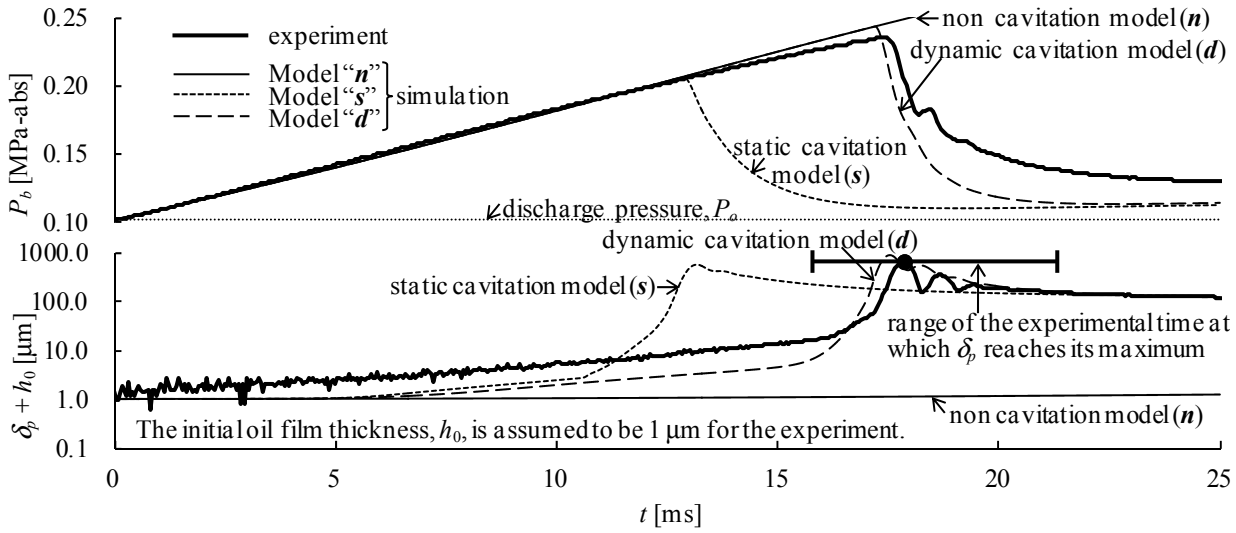

Figure 4: Bore pressure and reed displacement on the port in the experiment and simulations using three cavitation models

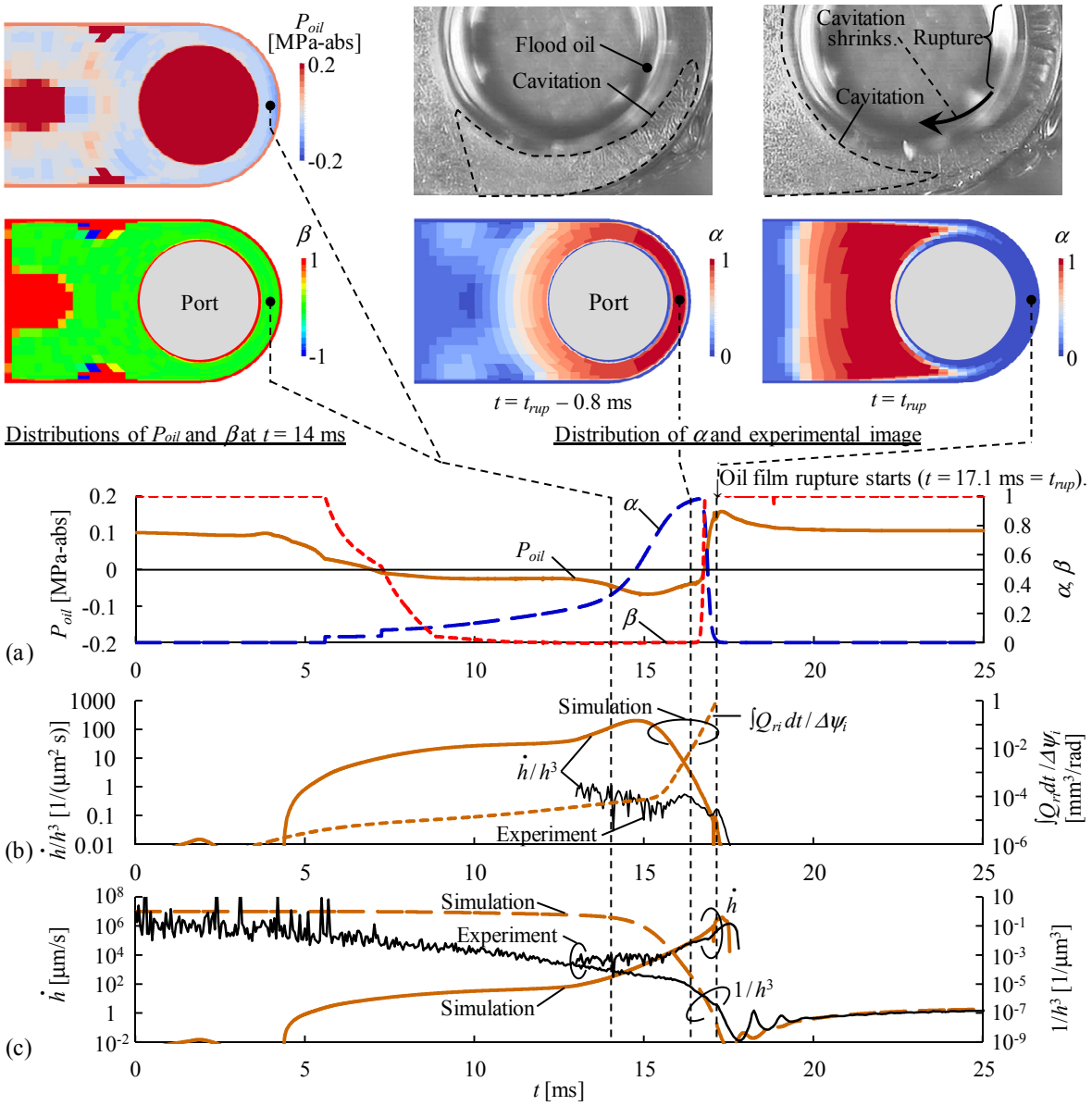

Figure 5: Time series and distributions of oil film quantities obtained by the simulation using Model "***d***" (Quantities at the tip side seal, ψ = 0°, r = 4.75 mm)

tip side seal) of oil film quantities obtained by the simulation using Model "***d***". In the simulation using Model "***d***", the absolute negative pressure (tensile in liquid) occurs in the oil film [Figure 5 (a) and the contour of P_{oil} (t = 14 ms)], while the minimum oil film pressure in model "***s***" is absolute zero. This difference on P_{oil} besides the difference on the delay time between Model "***s***" and Model "***d***" in Figure 4 indicates that the absolute negative pressure in the oil film must be taken into account in order to reproduce the experimental delay time quantitatively. This agrees the fact that the absolute negative pressure has been measured in the oil film under negative squeeze motion in previous experimental works (Kuroda, S., Hori, Y., 1978, Sun *et al*., 2008).

As shown in Figure 5 (a), void fraction, α, rapidly increases and decreases just before the oil film rupture. The rapid increase of α agrees the cavitation images captured in the experiment (Yoshizumi *et al*., 2012), and the rapid decrease also agrees the experimental images shown in Figure 5 (Cavitation shrinks in 0.8 ms.). As shown in the contour of β in Figure 5 (t = 14 ms), β becomes near zero in almost all of the area where bubbles grow ($P_{oil} < 0$). β being near zero means that the bubble growth occupies the volume change in the oil film and prevents the oil film

pressure, P_{oil}, from falling [see Equation (19)].

The accumulated flow volume toward radial outward, $\int Q_{ri}\, dt$ [Equation (24)], at the tip end of the seal in the simulation is shown in Figure 5 (b). The flow rate, Q_{ri}, i.e., the increase rate of $\int Q_{ri}\, dt$, is very small during stiction (t < 15 ms), and $\int Q_{ri}\, dt$ rapidly increases just before the oil film rupture (blow-by). This agrees oil film images captured in the experiment in that the gas does not infiltrate into the seal and the flood oil exists around the seal (along the port edge as well as the outer edge) until the oil film ruptures (Yoshizumi *et al*., 2012). The rapid increase of $\int Q_{ri}\, dt$ [Figure 5 (b)] synchronizes with the recovery of P_{oil} [Figure 5 (a)]. This means that the oil flows into the film by the negative squeeze motion during stiction (t < 15 ms), and the flow pattern changes to the one way flow towards the radial outward due to the recovery of P_{oil} just before the oil film rupture.

Here we consider the mechanism of the recovery of P_{oil} that leads to the oil film rupture. Being based on Equation (14), $\dot{h}/h^3$ is considered to be the source term of P_{oil} falling. Figure 5 (b) also shows the term, $\dot{h}/h^3$, and Figure 5 (c) shows $\dot{h}$ and $1/h^3$. The change in P_{oil} [Figure 5 (a)] synchronizes with the change in $\dot{h}/h^3$ [Figure 5 (b)]. This means that the recovery of P_{oil} is caused by the decrease of $\dot{h}/h^3$. Furthermore, Figure 5 (c) indicates that the decrease of $\dot{h}/h^3$ is caused by the decrease of $1/h^3$ (increase of h) that excels the increase of $\dot{h}$. Then, the direct cause of the recovery of P_{oil} is the increase of h. As for cavitation, Figure 4 indicates that the reed displacement, δ_p, in Model "***n***" does not increase while displacements in Model "***s***" and in Model "***d***" increase. This means that cavitation promotes the reed deformation separating from the seat and thereby the increase of h.

4. CONCLUSIONS

The dynamic cavitation model which simulates the absolute negative pressure in the oil film by the bubble growth model is required in order to reproduce the experimental delay time quantitatively. The simulation shows the mechanism of the oil film rupture (valve opening), i.e., the cavitation bubbles promote the increase of the oil film thickness during the stiction and the increased oil film thickness causes the recovery of the oil film pressure, and the subsequent blow-by flow (oil film rupture).

NOMENCLATURE

A_p, A_{p1}, A_{p2} flow areas at throats and the valve
$[C]$ damping matrix of the reed
C_d, C_{d0}, C_{d1}, C_{d2} flow coefficients at throats and the valve
D_p port diameter of the valve
F_g gas force acting on the reed ($\{F_g\}$ is the vector of the lumped forces on port nodes of the FEM reed model.)
$\{F_{oil}\}$ vector of lumped forces on FEM reed nodes caused by the pressure difference, $P_{oil} - P_o$
$f_r(z_r)$ probability density function of z_r (f_r is Gaussian in this research.)
H reed thickness
h oil film thickness (distance between averaged lines of the roughness of surfaces, $h = h_0 + \delta$)
$\overline{h}_T$ local film thickness
$[K]$ rigidity matrix of the reed
ℓ_d damping length of the reed valve
$[M]$ mass matrix of the reed
$\dot{m}_0$, $\dot{m}_1$, $\dot{m}_2$, $\dot{m}_v$ mass flow rates at throats and the valve
m_g mass of the dissolved gas in one bubble
N number of bubbles per unit contact area
P pressure (absolute value)
P_{cav} minimum oil film pressure for the Reynolds' condition
$P_{cav\ onset}$ oil film pressure at which the bubble growth onsets
P_{oil} oil film pressure (P_{oil} is set to P_o at $t = 0$.)
P_v saturated vapor pressure of the oil
Q_r volume rate of the oil in the r direction
R_g gas constant
r radial coordinates on the port
r_b the bubble radius
r_{bmin} the minimum limit of r_b
T temperature
t time (The origin is set as $t = 0$ at $P_b = P_o$.)
u_v inviscid gas flow velocity at the valve throat
V volume
V_{eoil} total oil volume adhered to the port edge at the initial stage
$\{X\}$ displacement vector of the reed
x, y, z Cartesian coordinates
z_r combined roughness
α void fraction of the oil film
β the volume rate fraction for liquid of the oil film
Γ diffusion coefficient of the dissolved gas in the oil

γ heat capacity ratio of the gas
δ out-of-plane displacement (displacement in z direction) of the reed (δ and $\dot{\delta}$ are set to 0 respectively at $t = 0$.)
δ_p δ on the port (averaged δ of the ϕ 5 mm area)
ϵ_r standard deviation of the combined roughness
ζ_j critical damping ratio of reed modes
η viscosity of the oil
Θ_v gas flow angle of the valve (z-dir.: 0, r-dir.: $\pi/2$)
κ_b coefficient of surface dilatational viscosity of bubbles
ν_{gb} polytropic index of the gas in bubbles
ξ_v velocity coefficient of the valve
ρ averaged oil film density or densities of the gas
ρ_{oil} density of the oil
ρ_v gas density at the valve throat
Λ_{va} position change ratio in the electro-magnetic valve
σ surface tension force of the bubble
ϕ_x, ϕ_y flow factors for the oil film flow ($\phi_x = \phi_y$ (isotropic roughness) in this reseach)
χ_g volume fraction of the gas in the oil
ψ circumferential coordinate around the port

Subscripts:
0 initial value (except $\dot{m}_0$)
1 middle chamber
b bore (except r_b)
g bubble
o discharge side
sup high pressure source

REFERENCES

Bauer, F., 1990, The Influence of Liquids on Compressor Valves, *Proceedings of the 1990 International Compressor Engineering Conference at Purdue*, p. 647-653.

Bukac, H., 2002, Understanding Valve Dynamics, *Sixteenth International Compressor Engineering Conference at Purdue*, C15-3.

Khalifa, H. E., Liu, X., 1998, Analysis of Stiction Effect on the Dynamics of Compressor Suction Valve, *Proceedings of the 1998 International Compressor Engineering Conference at Purdue* , p. 87-92.

Kuroda, S., Hori, Y., 1978, An Experimental Study on Cavitation and Tensile Stress in a Squeeze Film (in Japanese), *Journal of Japan Society of Lubrication Engineers*, Vol. 23, No. 6, p. 436-442.

Natsumeda, S., Someya, T., 1990, The Effect of the Surface Dilational Viscosity to the Negative Pressure in the Oil Film of Journal Bearing, *Proc. the Japan International Tribology Conference*, p. 1617-1622.

Patir, N., Cheng, H. S., 1978, An Average Flow Model for Determining Effects of Three-Dimensional Roughness on Partial Hydrodynamic Lubrication, *Transactions of the ASME*, *Journal of Lubrication Technology*, Vol. 100, p. 12-17.

Pizarro-Recabarren R. A., Barbosa Jr, J. R., Deschamps C. J., 2012, Modeling the Stiction Effect in Automatic Compressor Valves, *21st International Compressor Engineering Conference at Purdue*, 1126, p. 1-9.

Sun, M., Zhang, Z., Chen, X., Wang, W., Meng, K., Sun, D. C., 2008, Experimental Study of Cavitation in an Oscillatory Oil Squeeze Film, *Tribology Transactions*, Vol. 51, Issue 3, p. 341-350.

Yamaguchi, A., Hayashi, K., Piao, H. C., 1983, Study on Contraction and Disappearance of a Bubble in Oils, *Bulletin of JSME*, Vol. 26, No. 216, p. 993-998.

Yoshizumi, F., Yoshida, K., Moroi, T., Tamano, S., Morinishi, Y., 2012, Experimental Study on Opening Delay of a Reed Valve for Compressors: Visualization of Oil Film Behaviors and Measurement of Valve Deformations in the Opening Process, *R & D Review of Toyota CRDL*, Vol. 43, No. 4, p. 81-92.

Yoshizumi, F., Kondoh, Y., Moroi, T., Tamano, S., Morinishi, Y., 2013a, Calculation for the Opening Delay of a Discharge Reed Valve in Compressors (Coupled Calculation Model of Valve Deformation-Gas Flow-Oil Film Flow) (in Japanese), *Transactions of the Japan Society of Mechanical Engineers*, *Series B*, Vol. 79, No. 806, p. 1985-2002 and Vol. 79, No. 808, p. 2885.

Yoshizumi, F., Kondoh, Y., Moroi, T., Tamano, S., Morinishi, Y., 2013b, Calculation for the Opening Delay of a Discharge Reed Valve in Compressors (Opening Mechanism Based on the Valve Deformation-Gas Flow-Oil Film Flow Behavior) (in Japanese), *Transactions of the Japan Society of Mechanical Engineers*, *Series B*, Vol. 79, No. 806, p. 2003-2018.